Hearing Research 301 (2013) 156–167

Contents lists available at SciVerse ScienceDirect

Hearing Research

journal homepage: www.elsevier.com/locate/heares

Research paper

Two-port network analysis and modeling of a balanced armature receiver

Noori Kim*, Jont B. Allen

Department of Electrical and Computer Engineering, University of Illinois at Urbana-Champaign, 1206 W. Green Street, 2137 Beckman Institute, 405 N. Mathews, Urbana, IL 61801, USA

ARTICLE INFO

Article history:
Received 20 September 2012
Received in revised form
9 January 2013
Accepted 7 February 2013
Available online 26 February 2013

ABSTRACT

Models for acoustic transducers, such as loudspeakers, mastoid bone-drivers, hearing-aid receivers, etc., are critical elements in many acoustic applications. Acoustic transducers employ two-port models to convert between acoustic and electromagnetic signals. This study analyzes a widely-used commercial hearing-aid receiver ED series, manufactured by Knowles Electronics, Inc. Electromagnetic transducer modeling must consider two key elements: a *semi-inductor* and a *gyrator*. The semi-inductor accounts for electromagnetic eddy-currents, the 'skin effect' of a conductor (Vanderkooy, 1989), while the gyrator (McMillan, 1946; Tellegen, 1948) accounts for the anti-reciprocity characteristic [Lenz's law (Hunt, 1954, p. 113)]. Aside from Hunt (1954), no publications we know of have included the gyrator element in their electromagnetic transducer models. The most prevalent method of transducer modeling evokes the *mobility method*, an ideal transformer instead of a gyrator followed by the dual of the mechanical circuit (Beranek, 1954). The mobility approach greatly complicates the analysis. The present study proposes a novel, simplified and rigorous receiver model. Hunt's two-port parameters, the electrical impedance $Z_e(s)$, acoustic impedance $Z_a(s)$ and electro-acoustic transduction coefficient $T_a(s)$, are calculated using ABCD and impedance matrix methods (Van Valkenburg, 1964). The results from electrical input impedance measurements $Z_{in}(s)$, which vary with given acoustical loads, are used in the calculation (Weece and Allen, 2010). The hearing-aid receiver transducer model is designed based on energy transformation flow [electric→ mechanic→ acoustic]. The model has been verified with electrical input impedance, diaphragm velocity in vacuo, and output pressure measurements.

This receiver model is suitable for designing most electromagnetic transducers and it can ultimately improve the design of hearing-aid devices by providing a simplified yet accurate, physically motivated analysis.

This article is part of a Special Issue entitled "MEMRO 2012".

Published by Elsevier B.V.

1. Introduction

A *transducer* converts energy from one modality to another. A hearing-aid receiver is an electromagnetic loudspeaker that converts an electrical signal to acoustical pressure. It is referred to as an electromagnetic transducer in part, because small magnets are involved. Since these miniature loudspeakers are widely used in modern hearing-aids, and remain one of the most expensive components of the hearing-aids, a detailed understanding of them is therefore critical to optimize their design.

There are two poorly understood elements of special interest in the electromagnetic transducer: the *semi-inductor* and the *gyrator*. The semi-inductor component is required to account for eddy-current diffusion (the 'skin effect'). In 1989, Vanderkooy demonstrated that, at high frequencies, the behavior of the impedance of a loudspeaker changes from the behavior of a normal inductor to that of a semi-inductor, because of the eddy current diffusing into the iron pole structure of the loudspeaker. Using a Bessel function ratio, Warren and LoPresti (2006) represented Vanderkooy's semi-inductor model as a 'diffusion ladder network,' a combination of resistors and inductors. In 2010, Weece and Allen used this representation in a bone driver model. After demagnetizing the bone driver, they established the $\sqrt{s}$ behavior and determined the ladder network elements from the measured electrical impedance of the transducer. Thorborg et al. (2007) also introduced a loudspeaker model with lumped circuit elements, including a semi-inductor.

In 1946, McMillan introduced the anti-reciprocal component as a network element. Two years later, Tellegen (1948) coined the

* Corresponding author.
E-mail address: nkim13@illinois.edu (N. Kim).

0378-5955/$ – see front matter Published by Elsevier B.V.
http://dx.doi.org/10.1016/j.heares.2013.02.007

term 'gyrator,' and categorized it as a fifth network element, along with the capacitor, resistor, inductor, and ideal transformer. Other than Hunt's 1954 publication, we remain unaware of any publications which implement anti-reciprocity in their electromagnetic transducer model using a gyrator.

Referring back to the original formulation of Wegel (1921), Hunt (1954) proposed the basic 2-port impedance matrix which converts electrical signals to mechanical force,

$$\begin{bmatrix} E(\omega) \\ F(\omega) \end{bmatrix} = \begin{bmatrix} Z_e(s) & -T(s) \\ T(s) & z_m(s) \end{bmatrix} \begin{bmatrix} I(\omega) \\ V(\omega) \end{bmatrix}, \tag{1}$$

where E is the voltage, I is the current, F is the force and V is the particle velocity. The direction of I and V is defined as into the network. This matrix involves an electrical impedance $Z_e = \frac{E}{I}|_{V=0}$, a mechanical impedance $z_m = \frac{F}{V}|_{I=0}$, and an electromagnetic transduction coefficient $T = \frac{F}{I}|_{V=0} = -\frac{E}{V}|_{I=0}$. We call Z_e, z_m, and T the *Hunt parameters*,[1] which are functions of the Laplace (complex) frequency $s = \sigma + j\omega$. When the two off-diagonal elements of Eq. (1) are equal, the system is reciprocal; if they are opposite in sign, the system is anti-reciprocal, which is a necessary condition of the electromagnetic transducer, due to Lenz's law. Eq. (1) is equivalent to the 'factored' ABCD (transmission) matrix of Fig. 1.

The impedance matrix (Eq. (1)) is useful when making measurements. For instance, system's electrical input impedance and output acoustic impedance (or output mechanical impedance) can be represented with the impedance matrix elements, Z_e and Z_a (or z_m). The ABCD matrix representation (Fig. 1) is useful for network modeling, but then may be transformed into an impedance matrix for experimental verification.

One may convert between an impedance matrix to an ABCD matrix using the relationship:

$$\begin{bmatrix} A & B \\ C & D \end{bmatrix} = \frac{1}{T_a} \begin{bmatrix} Z_e & \Delta_Z \\ 1 & Z_a \end{bmatrix}, \tag{2}$$

where $\Delta_Z = Z_e Z_a + T_a^2$,and T_a is the acoustic transduction impedance (Van Valkenburg, 1964). Inverting the acoustical and electrical variables in Eq. (2) gives the inverse ABCD system:

$$\begin{bmatrix} P(\omega) \\ U(\omega) \end{bmatrix} = \frac{1}{\Delta_{ABCD}} \begin{bmatrix} -D(s) & B(s) \\ C(s) & A(s) \end{bmatrix} \begin{bmatrix} E(\omega) \\ I(\omega) \end{bmatrix}, \tag{3}$$

where $\Delta_{ABCD} = DA + BC = -1$, due to anti-reciprocity. Eq. (3) allows one to calculate the Thevenin pressure or Norton velocity in terms of the electrical input.

In the electromagnetic transducer models of both Weece and Allen (2010) and Thorborg et al. (2007), an ideal transformer was used to convert electrical current into mechanical force (or acoustical pressure) of the transducer. As described in Beranek (1954), the mobility strategy (along with the impedance or admittance analogy) is appropriate to represent electrical to mechanical transduction when modeling anti-reciprocal electromagnetic transducers using an ideal transformer. This mobility method fails to provide an intuitive explanation of the 'anti-reciprocity' characteristic of the electromagnetic transducer, which follows from Maxwell-Faraday's law and Lenz's law. Both the impedance and the mobility methods are mathematically equivalent, meaning one can choose either method to describe the system. However including the gyrator in transducer models allows for an intuitive yet accurate interpretation of physical properties. For example, when using a gyrator to represent the mechanical and electrical transformation, stiffness can be represented as a capacitor and mass as an inductor in the series combination. Given the mobility (dual) network, it is necessary to swap the inductor and capacitor, placing them in parallel combination. Thus we feel that this dual network is less intuitive for understanding the system.

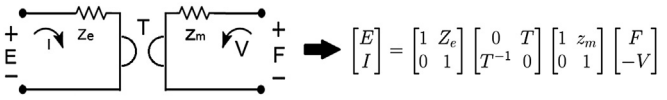

Fig. 1. Schematic representation of an electro-magnetic transducer and the equivalent factored ABCD matrix representation. The electrical and mechanical sections are coupled with a gyrator. Eq. (1) is the equivalent impedance matrix representation (Hunt, 1954).

1.1. A balanced armature receiver

The Knowles Electronics[2] ED series receivers shown in Fig. 2(a), including the ED7045 and ED1913, are balanced armature receivers (BAR),[3] widely used in hearing-aids. The ED receiver is $6.32 \times 4.31 \times 2.97$[mm] in size. These receivers consist of a coil, armature, two magnets, and a diaphragm. Unlike the alternative moving-coil drivers, the coil of the BAR has a fixed position (does not move) (Jensen et al., 2011), thereby reducing the mass and providing more space for a much longer coil. As the result of the lower mass, the BAR frequency response is higher, and due to the greater coil length, the sensitivity (T) is greater. The armature used for the ED7045 is an E-shaped metal reed (Bauer, 1953), whereas a U-shaped armature is widely used for the telephone instruments (Mott and Miner, 1951). Both shapes have advantages and disadvantages. For example, the U-shape armature has better acoustic performance (i.e., wide band frequency response) while the E-shaped armature lowers the vibration of the body more effectively. The armature is placed through the center of the coil and in between two magnets, without touching them. The movement of the armature is directly connected to the diaphragm through a thin rod (Fig. 2 (a)).

1.2. Sensitivity analysis of ED series SPICE model

Fig. 3 shows the Knowles Electronics commercial SPICE circuit model (Killion, 1992). This SPICE model contains a gyrator and is meant to be equivalent to the physical system, but does not accordingly represent the system in an one-to-one physical manner.

In order to fully understand each component, we implemented the Knowles PSpice model in Matlab using transmission matrices. Unlike PSpice, Matlab provides a more flexible platform for a matrix model manipulation. Matlab does not critically depend on the user's operating system (Knowles' PSpice model is inflexibly tied to both the Cadence Orcad Schematics and Capture, and Windows XP). PSpice requires a DC path to ground from all nodes, thus R1, RK512, RK513, and RK514 components have been added for this purpose.

We then performed a *sensitivity analysis* on the Matlab model by changing each component value by ±20% to determine those components for which the output changed by less than −50[dB], within the frequency range of 0.1–10[kHz]. Once the small effect components were determined, we removed the components from

[1] Wegel (1921) was the first to define Eg. 1 in this form, so perhaps we should call these the Wegel parameters.

[2] Knowles Electronics, Itasca, IL (http://www.knowles.com).

[3] BAR: Balanced Armature Receivers.

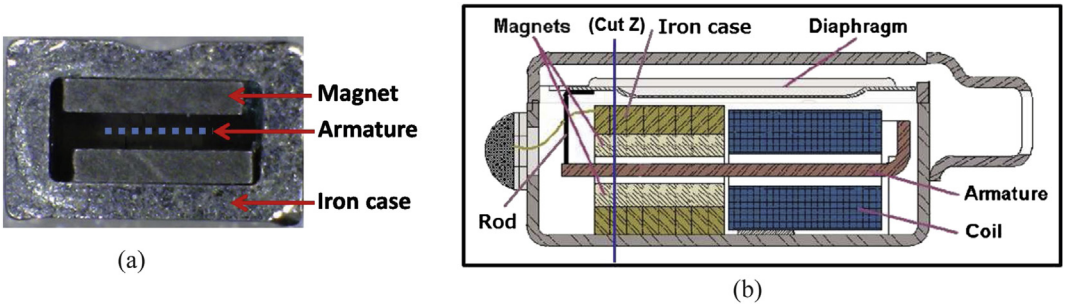

Fig. 2. (a): The picture of the BAR at 'Cut Z' line in panel (a). There is a space for the armature to vibrate vertically between the magnets. Magnets are sandwiching the armature (a blue, dotted line). A laminated iron case surrounds the magnets and the armature. (b): A schematic of a BAR. An electrical current in the coil comes from the transducer's electrical input terminals; the current induces a Lorentz force on the armature via the induced magnetic field. (Modified from Knowles documentation about ED receiver series.) Note that the port location of ED7045 receiver is rotated 90° to the longer side, which is different from this general scheme of the ED series. (a) The cross-section view of the receiver (b) The structure of ED7045 receiver.

the original PSpice design for a further Matlab analysis. To compare the difference between the original and the reduced components condition, we calculate each error computed across frequencies,

$$e(f) = \frac{|\text{'Original'} - \text{'Smalleffect'}|}{|\text{'Original'}|}, \tag{4}$$

where f is frequency. Our Matlab simulation result is shown in Fig. 4(a) with the CMAG value defined in the PSpice circuit (in Fig. 3, CMAG = 0.92e-7). The 'Original' simulation contains all circuit elements without any modification, whereas the 'Small effect' simulation excludes the small effect components in Fig. 3. The PSpice sensitivity analysis for the semi-capacitor is performed using Knowles PSpice library for the CMAG component[4] shown in Fig. 4(b). The most important result of this sensitivity analysis was that the semi-capacitor in the PSpice model is one of these 'small effect' components.

Using a series semi-capacitor on the right side of the gyrator is mathematically equivalent to using a shunt semi-inductor on the left side of the gyrator, because of mobility and impedance analogies. However, ideally, circuit elements should be properly associated with their physical properties. It is important to take advantage of using a gyrator to describe the anti-reciprocity for a physically intuitive model of the system. The gyrator is the bridge between the electrical and mechanical systems. For this reason the coil of the receiver should be represented on the electrical side. This realization further motivated our objective to design a simplified and rigorous BAR model.

The remainder of our analysis is structured as follows: Section 2 introduces the theoretical concepts, specifically related to designing electro-magnetic transducer models. Section 3 presents the experimental methods used in the present study. Section 4 includes the results from the experiments. Hunt's parameters are derived via electrical impedance measurements to establish the fundamental properties of the transducers. We present the final proposed transducer model in Section 5, which is followed by our model verification via experimental comparison in Section 6.

2. Theories

2.1. Two-port network theory

Two-port networks (Eq. (1)) based on Ohm's law generalize the one-port Thevenin/Norton model and are used to characterize linear transducers (Hunt, 1954; Van Valkenburg, 1964; Wegel, 1921).

Carlin and Giordano (1964) identified six properties of two-port networks: *1. Linearity* – A network is linear if the scaling and addition of the input causes the same effect on the output. *2. Time-Invariance* – In a time-invariant network, shifting a signal in time does not affect the characteristics of the network. *3. Passivity* – A network is passive if its components do not contain a power source. *4. Causality* – A causal network's output does not predict the input. *5. Real-Time Function* – A network must respond to a real time-signal with a real output response. *6. Reciprocity* – A two-port network is reciprocal if and only if the off-diagonal elements of the impedance matrix are equal.

Based on McMillan (1946) and Hunt (1954), a moving-armature electromagnetic transducer can be approximately considered to be a linear, time-invariant, passive, causal, real-time and anti-reciprocal system (the off diagonal elements if Eq. (1) have opposite signs). Note that a semi-inductor impedance $\sqrt{s}$ is linear, since it can be transformed into the time domain response via the inverse Laplace transform (a linear causal operator) according to

$$\frac{1}{\sqrt{s}} \leftrightarrow \begin{cases} 0 & t \le 0 \\ \dfrac{1}{\sqrt{\pi t}} & t > 0 \end{cases}.$$

2.2. Two-port relationship: impedance and ABCD (transmission) matrices

The two-port 'electro-acoustic' transducer equation can alternatively be represented in ABCD matrix form, as given by Eq. (5) and Eq. (1). The fundamental difference of the two matrix systems lies in the coupling of the 'electro-acoustic' transducer, between the mechanical and the acoustic signals (i.e., ±T(s) of Eq. (1)). Specifically, the electrical input parameters E and I on the left side of the network and Eq. (5) are expressed in terms of the acoustical variables, the pressure P and the volume velocity U, on the right side of the network (or alternatively F and V for an 'electro-mechanical' transducer), via the four frequency dependant parameters A, B, C, and D:

$$\begin{bmatrix} E(\omega) \\ I(\omega) \end{bmatrix} = \begin{bmatrix} A(s) & B(s) \\ C(s) & D(s) \end{bmatrix} \begin{bmatrix} P(\omega) \\ -U(\omega) \end{bmatrix}. \tag{5}$$

As shown in Fig. 1, each network element may be represented with a 2 by 2 ABCD matrix, with the volume velocity U defined as flowing out of the element (resulting in the '-' sign). Thus multiple

[4] This simulation result was provided by Knowles Electronics.

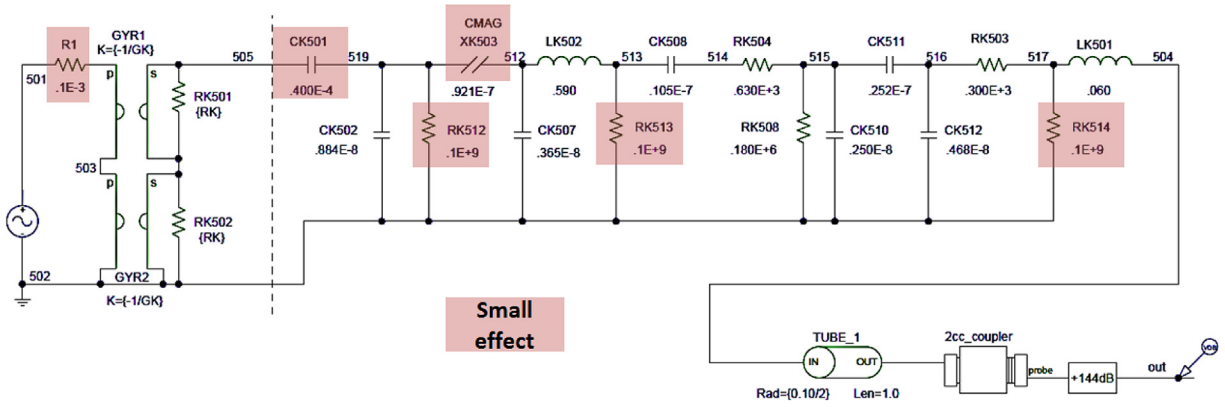

Fig. 3. Knowles PSpice model of the ED receiver: The refined PSice circuit model of ED receiver by reducing 'small effect' components which are marked in red. R1, RK512, RK513, and RK514 resistors were added to maintain DC stability of PSpice. Note that the Spice model represents all ED series receivers, including ED7045, ED1744, ED1913, and etc., such that specific parameter value of components vary for each specific receiver.

elements' matrices can be 'chained' (i.e., factored) in accordance with different combinations of the elements (i.e., series or shunt). This allows one to represent the network using matrix multiplication. Therefore, when we transform the ABCD matrix to an impedance matrix, it is necessary to force a negative sign for the volume velocity to maintain consistency.

Based on Eq. (5), we can define 'open circuit' and 'short circuit' conditions for both the acoustical and the electrical impedance. Thus, the acoustical impedance (Z_a) and electrical impedance (Z_e) is defined as:

$$Z_a(s) \equiv \frac{P(\omega)}{U(\omega)} = \left.\frac{D(s)}{C(s)}\right|_{I=0} = \left.\frac{B(s)}{A(s)}\right|_{E=0} \tag{6}$$

$$Z_e(s) \equiv \frac{E(\omega)}{I(\omega)} = \left.\frac{A(s)}{C(s)}\right|_{U=0} = \left.\frac{B(s)}{D(s)}\right|_{P=0}. \tag{7}$$

As described earlier, the corresponding Hunt parameters, Z_e and Z_a for acoustics (or alternatively z_m for mechanics), are defined under the open circuit condition, $I = 0$ and U (or V) $= 0$, respectively. The specific methods and results are discussed in Section 3 and 4.

2.3. Gyrator and anti-reciprocity

When electric field ($\overline{E}$) is induced by the changing magnetic field ($\overline{B}$), the relationship between those two fields is described by the differential form of the Faraday-Lenz law:

$$\nabla \times \overline{E} = -\frac{d}{dt}\overline{B}. \tag{8}$$

Applying Stoke's theorem over the area S_a, bound by contour C, results in the integral form of the above law:

$$\oint_C \overline{E}\cdot\overline{dl} = -\frac{d}{dt}\int_{S_a} \overline{B}\cdot\overline{dS} = -\frac{d}{dt}\varphi(t), \tag{9}$$

where $\phi(t)$ is magnetic flux in time domain. This equation tells us that the measure of the induced (rotation) electric field results in an equal negative time rate change of the magnetic flux. Note that the

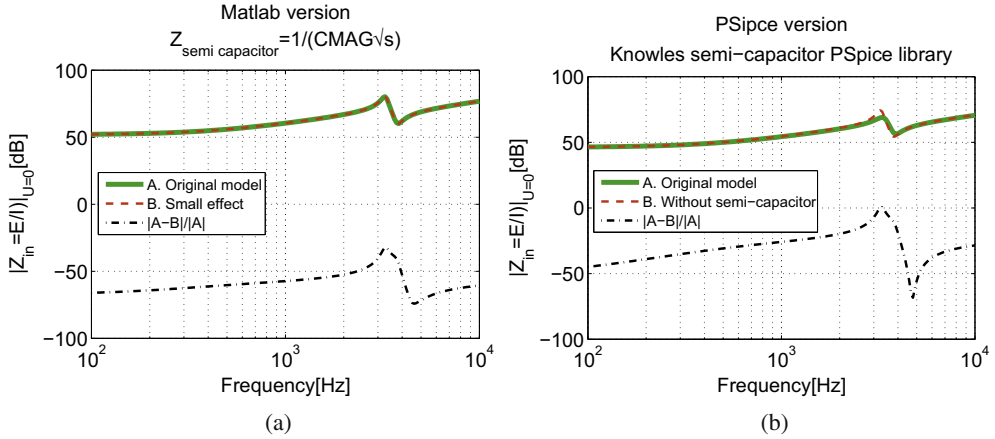

Fig. 4. The simulated electrical input impedance' magnitude, $|Z_{in}|$, in dB scale. (a) shows the sensitivity analysis using Matlab based on Fig. 3 where $s = j\omega$. The 'A. original model' and the 'B. Small effect' conditions are marked with a thick green line and a dashed red line, respectively. The 'B. Small effect' is the simulated result when all 'small effect' components in Fig. 3 are removed in the original PSpice circuit. It represents summed-up sensitivities of 'small effect' components in Fig. 3. (b) represents the sensitivity of the CMAG component only. This analysis is provided by Knowles Electronics using their PSpice library for the CMAG component (This result is plotted in Matlab but the data is acquired via PSpice simulation). Similar to the (a), 'A. Original model' shows the PSpice simulation including all components in Fig. 3, whereas 'B. Without semi-capacitor' simulates the original PSpice circuit only without the semi-capacitor. For both simulations (a) and (b), the difference between the original response and the reduced response is calculated based on Eq. (4) shown as black dashed line. (a) Matlab simulation (b) PSpice simulation.

negative sign comes from Lenz's law due to the conservation of energy. This mutual dependance of the two fields with a negative sign is the anti-reciprocal gyrator relationship.

A gyrator is required when quantifying the anti-reciprocal coupling between the electric and the magnetic fields (Tellegen, 1948), as shown in Fig. 1 (Hunt, 1954). The impedance matrix and the corresponding transmission matrix of a gyrator are:

$$\begin{bmatrix} E \\ F \end{bmatrix} = \begin{bmatrix} 0 & -T \\ T & 0 \end{bmatrix} \begin{bmatrix} I \\ V \end{bmatrix}, \begin{bmatrix} E \\ I \end{bmatrix} = \begin{bmatrix} 0 & T \\ 1/T & 0 \end{bmatrix} \begin{bmatrix} F \\ -V \end{bmatrix}. \tag{10}$$

To account for the mechanic–acoustic transition in electro-acoustic transducers, the force and particle velocity in the mechanical part are transferred into the pressure P and the volume velocity U of the acoustical part. Physically, the diaphragm or speaker cone vibration determines the air particle movements associated with volume, which is the source of the radiated pressure and the loaded impedance. Because of this radiation, the mechanical transduction T must be augmented by an acoustic propagation delay in the electro-acoustic circuit, namely

$$T_a(s) = Te^{-s\tau_0}, \tag{11}$$

where including an acoustic system delay (τ_0). Note that T_a represents a transduction relationship of the electro-acoustic transducers, from electric to mechanic to acoustic, whereas the gyration coefficient T only considers the electric to the mechanical (or magnetic) conversion. In the case of a moving-coil loudspeaker, T is defined as B_0l, namely, the product of the magnetic field (B_0) and the length of the wire coil (l) (Dodd et al., 2004; Thorborg et al., 2007; Hunt, 1954).

From Eq. (10), we can have two relationships:

$$E = -TV, \tag{12}$$

$$F = TI. \tag{13}$$

According to Hunt (see also Beranek), these two equations can be explained using the magnetic term of the Lorentz force, that is $T = B_0l$. Physically, Eqs. (12) and (13) can be understood as generator and motor components, respectively. Eq. (12) relates Faraday's induction law, Eq. (9), where the voltage E is defined as

$$E = -\int_c^d \overline{E}\cdot\overline{dl}, \tag{14}$$

where $\overline{E}$ is the electric field and the voltage is E. Note that the integral path is taken from negative terminal (c) to the positive terminal (d) of $\overline{E}$.

Eq. (13) follows Ampere's law. A wire carrying current $\overline{I}$ experiences a force $\overline{F}$ with the magnitude of B_0lI. This equation can be expressed as

$$\overline{F} = l\overline{I} \times \overline{B_0}, \tag{15}$$

where $\overline{F}$ is the magnetic net force on a stationary wire assuming a static B_0. Thus every electromagnetic transducer, including both the BAR and the moving-coil speaker, satisfies the condition that $T = B_0l$. Furthermore, we may infer the direction of the force on the armature, which is always perpendicular to both the current and the magnetic field (normal to the surface of the armature plate).

2.4. An alternative theory for T

Following Hunt's 1954 chapter 7, Jensen et al. (2011) derived a non-linear time-domain BAR model for T. Based on their theory, the input force of the moving-armature transducer system employs 'the tractive force' which attempts to minimize the air gap between the armature and the magnet. According to this theory

$$F = \frac{S_a\overline{B}^2}{2\mu_0} = \frac{\Phi_0^2}{2\mu_0 S_a}, \tag{16}$$

where $\overline{B}$[Wb/m^2] is the magnetic field across the air gap, S_a[m^2] is the transverse area of the armature with the permanent magnet, μ_0 is the permeability in free space ($4\pi 10^{-7}$[H/m]), and $\Phi_0 (= \overline{B}_0 S_a)$[Wb] is the total magnetic flux in the air gap (Hunt, 1954; Jensen et al., 2011).

2.5. Semi-inductor

Vanderkooy (1989) first identified the electrical impedance representation of the semi-inductor due to the eddy current as proportional to $\sqrt{s}$. A simple impedance formula of the semi-inductor is derived with the assumption that the length of a coil sheet is infinite. Neglecting the radius of the coil and the air gap between the magnetic material and the wire,

$$Z_{semi} = n^2\sqrt{\frac{\mu s}{\sigma}} = K\sqrt{s}, \tag{17}$$

where K is semi-inductance per unit length in semi-henrys, n is the number of coil winding turns of wire, μ is the iron's permeability, and σ is the conductivity of the iron armature.

Semi-inductors, which result from magnetic diffusion, are not commonly found in circuit analysis. However, it is a key element in characterizing the 'eddy-current' (skin effect) in electromagnetic models, such as loudspeakers. In a BAR, the eddy current is distributed through the surface of the armature, as well as on the cross section of the laminated iron box which surrounds the magnets (Fig. 2). In a dynamic loudspeaker, on the other hand, the coil is directly connected to the diaphragm and the eddy-current is distributed through the surface of an iron core (a pole-piece structure).

Warren and LoPresti (2006) noted that the Bessel function ratio in the Vanderkooy model (1989) can be expanded as a continued fraction expansion, into a diffusion ladder network, so that the electrical impedance can be represented by the circuit shown in Fig. 5. The semi-inductor model includes two parameters: the diffusion resistance R, and the shunt diffusive inductance L which can be represented by the physical characteristics of the transducer. From Warren and LoPresti (2006) and Vanderkooy (1989), R and L are given by

$$R = \frac{4\pi n^2 l}{\sigma}, \quad L = \mu l n^2 \pi r_0^2, \tag{18}$$

where n is the number of coil windings, l is the coil length, σ is the conductivity of the pole structure, μ is the permeability of the pole structure, and r_0 the coil radius.

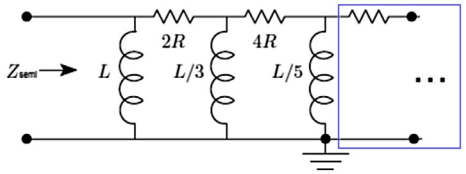

Fig. 5. Semi-inductor lumped circuit model via ladder network. Circuit diagram of the electrical impedance of the semi-inductor model is defined by the ladder network resistance factor R and shunt inductance factor L (Weece and Allen, 2010).

Although the combination of the resistor and the inductor should extend to infinity (more resistor–inductor pairs), these can only affect higher frequencies (i.e., Fig. 5 is a sufficient low frequency approximation). As shown in Fig. 5, Weece and Allen (2010) determined only 5 elements (L, 2R, L/3, 4R, and L/5), and compared the network to the demagnetized condition of their bone driver transducer. Demagnetizing the transducer ($T = B_0 l = 0$) is mathematically equivalent to the open circuit condition (i.e., $U = 0$).

3. Methods

Three different experiments were conducted in this study. First, we calculate the Hunt parameters of a BAR from electrical input impedance measurements (Appendix A.). The calculation of Hunt parameters may be considered as a two-port Thevenin calibration of the receiver, since Z_e, T, and Z_a characterize the initial electrical, acoustical and transfer properties of the unloaded receiver. Second, we measure of the receiver's diaphragm velocity in vacuum using a laser. This procedure was needed to verify the mechanical and electrical parts of the model. The last step is the pressure measurement of the receiver using an ER7C probe microphone, (Etymotic Research). The resulting Thevenin pressure of the receiver from our transducer model and Hunt parameters is compared with this experimental pressure data. The detail of this result is discussed in Section 6 (model verification).

3.1. Electrical input impedance measurements for the Hunt parameter calculation

Step 1 of calculating Hunt's parameters of the receiver requires a system for measuring electrical impedance as a function of frequency. As shown in Fig. 6, all stimulus signals were generated using a laptop sound card so that voltages could be recorded. The stimulus waveform was a 24-bit, 2048-point frequency-swept chirp with a sampling rate of 48[kHz]. The signal-to-noise ratio (SNR) was improved by looping the chirp and averaging between 10 and 100 consecutive frames, depending on the required SNR. The $\leqq 1$ V chirp signal from an Indigo sound card (Echo Audio) was sent to the receiver, which was in series with a known reference resistor R (1000[Ω], Fig. 6). The resistor was located between one of the receiver's terminals and the sound source ground. The measured electrical input impedance is expressed as:

$$Z_{\text{in}} = \frac{E_A - E_B}{I} = \frac{E_A - E_B}{E_B/R} = R\left(\frac{E_A}{E_B} - 1\right). \tag{19}$$

As shown in Fig. 7, eight different acoustic loads were attached to the end of the receiver output and eight corresponding electrical input impedances were recorded. Six of the seven tubes (excluding the longest length 6.11[cm]) were used in the experiments: 0.25, 0.37, 0.88, 1.24, 2.39 and 3.06[cm]. The inner diameter of the tubes was about $\approx$1.5[mm], which is similar to the outer diameter of the ED receiver port. As three different measurements were required to

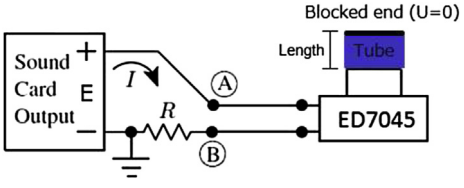

Fig. 6. Experimental setup for the electrical input impedance measurement. Where E is the voltage, I is the current, and R is a reference resistance. We varied the experimental condition by changing length of a blocked tube and measured the voltage at two points (A, B) Denoted as E_A and E_B.

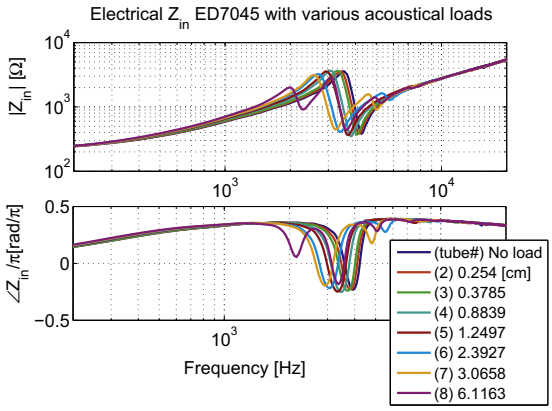

Fig. 7. Measured Z_{in} of ED7045 with the eight acoustical load conditions, blocked cavities. Different lengths of the tubes are used to vary the acoustical load. Three different known electrical input impedances are selected to calculate Hunt's parameters.

calculate the three unknown Hunt parameters (Z_e, Z_a, T_a) (Weece and Allen, 2010), three out of six tubes with different lengths were selected, resulting in $6C3 = 20$ possible combinations of the Hunt parameters. The results from every possible combination are not discussed in this paper; rather, we focus on the four calculated sets of Hunt parameters. We categorized our testing tube lengths into short, medium and long tubes, and picked one of each to make a set of three tubes. An open circuit condition (the volume velocity, U, is zero.) was applied, as the ends of the tubes were blocked for the experiment. The characteristics of the resulting derived Hunt parameters are discussed in Section 4.

When the acoustic load impedance is unblocked, a small second resonance (SR)[5] appears around 7.6[kHz], following the first resonance (FR)[6] at 2.5[kHz], as shown in Fig. 8(a) (green). In fact, a very small SR appears in *every* case in the figure, as clearly seen in the polar plot, Fig. 8(b). The SR of the blocked case (red) is not obvious in the magnitude plot, but one sees the SR location from the phase in the polar data. Note that a 'loop' in the polar data corresponds to the SR in these magnitude data. The vacuum data (blue) shows the biggest FR in magnitude (the largest circle in the polar plot), and the FR locates at the lowest frequency among all the other cases. Compared to the unblocked case (red), the SR frequency of the other two cases (blocked and vacuum) is above the frequency range of reliable measurements. In detail, it has almost an octave difference ($\text{SR}_{\text{unblocked}} \approx 7.6[kHz]$, $\text{SR}_{\text{vacuum}} \approx 13.3[kHz]$, $\text{SR}_{\text{blocked}} \approx 15.7[kHz]$). In addition, the size of $\text{SR}_{\text{blocked}}$ is insignificant. For these reasons, we have ignored the SR effect in our model analysis of the BAR model.

3.2. Laser vacuum measurements

Fig. 9 describes the experimental setup of the laser mechanical velocity measurement in the vacuum environment. In preparation for the laser measurement, a portion of the transducer's case was carefully removed using a dental drill, to expose the diaphragm. A thin plastic window was glued on, to reseal the case. The laser beam is finely focused on the diaphragm through the window. The measurement was made where the driver rod (Fig. 2) connects to the diaphragm. For the vacuum condition, air inside the receiver was evacuated prior to measurement. The ambient pressure was maintained at less than 0.003[atm] during these measurements. The custom built vacuum system was used with a 'Sergeant Welch'

[5] SR: Second Resonance.
[6] FR: First Resonance.

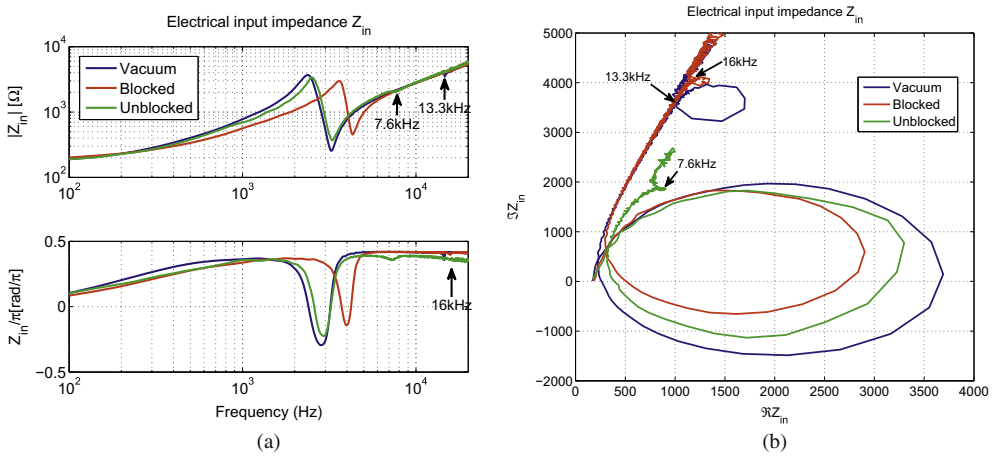

Fig. 8. This plot shows the electrical input impedance of the ED7045 receiver in blocked/unblocked port, and vacuum conditions. In the unblocked receiver port case, the FR moves to lower frequency (2.5[kHz]) compared to the blocked case, 3.8[kHz]. The FR in vacuum is at the lowest frequency, 2.3[kHz]. The frequency locations of SR for each curve are indicated by arrows in the figures. (a) Magnitude and phase of the electrical input impedance, (b) Polar plot of the electrical input impedance ($\Re Z_{in}$ vs $\Im Z_{in}$). Note that above 5[kHz], the phase of Z_{in} in (a) approaches $\approx 4\pi$[rad]. Thus in (b), the curves merge at a fixed angle as $\omega \to \infty$. (a) Magnitude and phase of Z_{in} of the ED7045 receiver (b) Z_{in} polar plot.

vacuum pump and a 10-inch bell-shaped jar. A 'Polytec OFV-5000 Vibrometer controller' was used with a 10x-lens on the laser. The calibration factor for the laser velocity was 125[mm/sec/volt]. As before, a chirp was used to measure the complex velocity frequency response.

3.3. Pressure measurements

The purpose of experiment three is to compare the output pressure to the model with $U = 0$. An ER-7C probe microphone (Etymotic Research) was used for the transducer pressure measurement. The probe tube was 0.95 OD × 0.58 ID × 76[mm], and made of medical grade silicon rubber. In fact, it is impossible to connect a microphone probe with a perfectly blocked receiver ($U = 0$) due to the finite load impedance of the microphone. The space between the microphone's tube and the port of the receiver is minimized, so the tube and the port do not touch each other. The real part of the characteristic impedance of a tube, Zc_{tube}, (without loss) is given by

$$Zc_{\text{tube}} = \frac{\rho c}{\text{Area}_{\text{tube}}}, \tag{20}$$

where ρ is the air density and c is the speed of sound ($1.21[kg/m^3]$ and 342[m/s] at 20°[C], respectively). The diameter, d, of the receiver's port and the microphone's tube are $d_{\text{receiver}} = 1.4[mm]$ and $d_{\text{mic}} = 0.58[mm]$, thus the area of the receiver's port is about 5.8 times larger than the microphone's. Adding more consideration of the length of both cases, $Zc_{\text{mic\_tube}}$ is much greater than $Zc_{\text{recever\_port}}$. Thus we assume that $Zc_{\text{mic\_tube}}$ has a negligible loading effect on the source impedance of the receiver. Recognizing these experimental limitations prior to comparing the measurement data to theoretical results should give us better understanding of the Thevenin pressure of the BAR.

Utilization of this experiment can be found in section 6.4 for comparing the model calculated Thevenin pressure (per voltage) to the experimental pressure measurement.

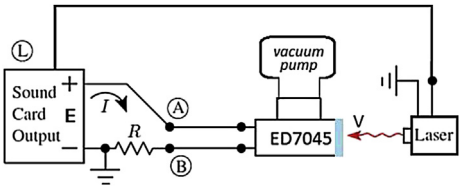

Fig. 9. Experiment setup for the laser mechanical velocity measurement in vacuum. The circled 'L' means an input from the laser system. The laser beam is focusing on the plastic window of the transducer to measure the diaphragm velocity (V).

4. Hunt parameters Z_e, Z_a, and T_a

4.1. Calculation

Z_e, Z_a and T_a are to be the estimated from Z_{in} given three different acoustic load conditions. Similar to Eq. (1), the BAR can be represented by its electro-acoustic impedance matrix, in terms of the port volume velocity U and pressure P, as

$$\begin{bmatrix} E(\omega) \\ P(\omega) \end{bmatrix} = \begin{bmatrix} Z_e(s) & -T_a(s) \\ T_a(s) & Z_a(s) \end{bmatrix} \begin{bmatrix} I(\omega) \\ U(\omega) \end{bmatrix}. \tag{21}$$

The acoustic load impedance Z_L is defined by Ohm's law as (U is defined as into the port)

$$Z_L \equiv \frac{P}{-U}. \tag{22}$$

Combining Eq. (21) and Eq. (22) and solving for U gives

$$U = \frac{-T_a I}{Z_L + Z_a}. \tag{23}$$

Replacing U in Eq. (21) gives an expression for the loaded electrical input impedance ($U \neq 0$)

$$Z_{\text{in}} \equiv \frac{E}{I} = Z_e + \underbrace{\frac{T_a^2}{Z_L + Z_a}}_{Z_{\text{mot}}}, \tag{24}$$

where Z_{mot} is denoted the *motional impedance* due to the acoustic load shown in the electric terminals (Hunt, 1954). Thus the Z_{in} obtained through measurements depends on the acoustic load, Z_L. Varying the acoustic load, which can be done by varying the length of the tube, gives different Z_{in} values (Fig. 7). The algebraic details are discussed in Appendix A.

4.2. Investigations

The calculated Hunt parameters of the BAR derived from various Z_{in} (Fig. 7) are shown in Fig. 11. Some considerations for the Hunt parameters of the BAR are as follows:

1. $\mathbf{Z}_e$: Compared to $Z_a(s)$ and $T_a(s)$, $Z_e(s)$ has the smallest dependency on the choice of load cavities (the three of six chosen load impedances: loads (2)–(7) in Fig. 7). Below 200[Hz], $Z_e(s)$ converges to a fixed resistance (ED7045: $\approx 195[\Omega]$). The frequency range between 0.5 and 2.5[kHz] is proportional to 's' (Z_e shows a constant slope in this frequency range). It is not clearly shown at frequencies below 10[kHz], however when the frequency increases more, the slope of Z_e approaches that of '$\sqrt{s}$'. Better evidence of '$\sqrt{s}$' domination at high frequency is shown in Section 6.2 in the polar plot. These frequency dependant impedance behavior (proportional to a constant, 's' and '$\sqrt{s}$') is determined by the coil properties, which are closely related the DC resistance, inductance and the semi-inductance. Note that Z_{in} (measured) $\rightarrow$ Z_e (calculated) as $U \rightarrow 0$.
2. $\mathbf{Z}_a$: For the frequencies below 2.5[kHz], Z_a is stiffness dominated (i.e., a capacitance), and between 2.5 and 4[kHz] it is dominated by the mass of the diaphragm and armature. Those properties determine the first anti-resonance (zero, near 2.5 [kHz]). The resonance (pole) at 3.7[kHz] is the frequency where the transfer impedance, T_a, is maximum. The pole of Z_e is also introduced in this frequency point. As T_a and Z_a are tied more closely, they move together when the set of Hunt parameter is changed while Z_e is almost identical over every set of the Hunt parameters (Fig. 13). Above 4[kHz] the transmission line and acoustic properties dominates given the small volume inside the receiver. Error above 6–7[kHz] is primarily caused by the experimental limitations, such as the manual manipulation of the tubes.
3. $\mathbf{T_a}$: It is nearly constant below 2–3[kHz] and is 4×10^5[Pa/A] at 1[kHz]. The phase shift in T_a is due to acoustic delay. Although the frequencies above 6[kHz] are obscured by the noise, T_a seems to behave as an all-pole function, which depend on the system delay τ. To account for this delay, a transmission line (Tx line) is added to the acoustic model, as shown in Fig. 12.

5. Results: proposed receiver model

Fig. 12 shows the final ABCD model. The electrical circuit elements are shown to the left of the gyrator. R_e is approximated to the DC resistance. The source of the armature movement is the Lorentz force ($F = \int J \times BdA$) due to the interaction of the current in the coil and the static magnetic field B_0 of the magnets. The current in the coil and the core of the E-shaped armature give rise to the inductance L_{em}, while the penetration of the magnetic field into the core induces an eddy current, depicted by a semi-inductor element K_1 in Fig. 12 (Vanderkooy, 1989). L_e represents any leakage flux, in air gap, which explains an additional small stored energy.

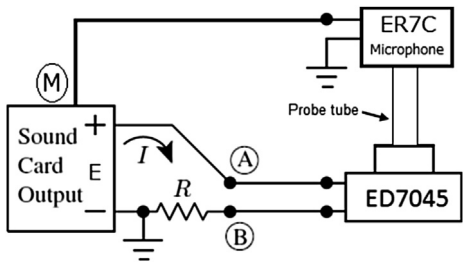

Fig. 10. Experiment setup for pressure measurement. The circled 'M' means an input from the ER7C microphone.

There should be a transition frequency, $f_t = 1/2\pi(K_0/L_0)^2$, between the inductor (L_0) and the semi-inductor (K_0). Since we used two inductors and one semi-inductor (total 3) for our receiver model, it is unclear exactly how to calculate the f_t from these components as we discussed in Section 4.2. However as shown in Fig. 14 (polar plot), the slope of the impedance is approaching $\sqrt{s}$ (45°) as ω increases. Based on Thorborg et al. (2007), the f_t of a dynamic loudspeaker is 100–200[Hz], which means the f_t for the balanced armature receiver is much higher than for the moving coil loudspeaker.

The gyrator relates the electrical and the mechanical sections with parameter $T = B_0 l$. The wire inside the ED7045 receiver is made of 49 AWG copper, which has a resistivity of 26.5[Ω/m]. Since the measured DC resistance of the receiver is around 190[Ω] we can calculate the length of the wire is approximately 7.1[m]. In general, the dynamic moving-coil speaker's l is shorter than the BAR's. Therefore we can expect a larger 'T' value for the BAR ($n \propto l$, $1/d_{\text{coil}}$).

To the right of the gyrator are the mechanical and acoustical sections of the transducer. We can simply describe the mechanical section as composed of a series combination of the armature and the diaphragm's stiffness, mass and damping. The transformer's coupling ratio of the acoustic side to the mechanical side is related to the diaphragm's area. The capacitor (C_a) and a transmission line in the acoustical part account for the back (rear) volume and sound delay. Because we are using a gyrator, the mobility analogy method is not used (Beranek, 1954; Hunt, 1954).

The Thevenin pressure of the BAR is defined given that the volume velocity (U) at the port is zero ('blocked' port), meaning the load impedance is set to ∞.

6. Verification of the transducer design

Several comparisons are made to verify that the transducer model (Figs. 11 and 12). First, the Hunt parameters are calculated from the model to support the transfer relation between electrical and acoustical parts (Section 3.1), as outlined in Appendix A. The mechanical part of the transducer model was verified by conducting laser mechanical velocity measurements in a vacuum condition (Section 3.2). Along with these results, we simulated the Thevenin pressure of the transducer from our model and compared the result to the pressure measurement (when $U = 0$) (Section 3.3). These three comparisons (electrical, mechanical, and acoustical) verify the transducer model (Fig. 12).

6.1. Hunt's parameters comparison

The Hunt parameters, from the model and the experimental calculation, are compared in Fig. 13. The discrepancies of Z_a above $6-7$[kHz] are presumably caused by the manual adjustment of the experimental conditions. This error is insignificant in Z_e. However the small noise in electrical impedance impacts the parameter estimation far from the electrical side. In other words, we can see the largest variation in acoustical parameter (Z_a), as the transition order goes from $Z_e \rightarrow T_a \rightarrow Z_a$.

Another interesting parameter is the resonant frequency. The frequency of the pole (f_p) for all figures looks almost identical: Z_e. Z_a and T_a slightly differ by the set, but the f_p of the two parameters occurs priory at the same location for the same set of Hunt parameters. The three parameters assume the zero-loaded condition which means, in theory, the f_p should be identical for all cases.

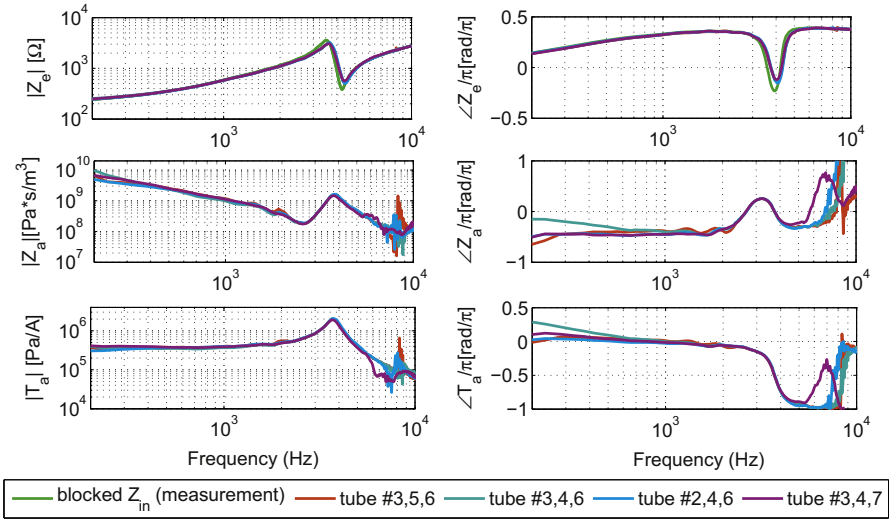

Fig. 11. Calculated Hunt parameters (Z_e, Z_a, and T_a) of the ED7045. Three measurements of Z_{in} with acoustic loads (indicated by number as shown in the legend) are required to find one set of the three Hunt parameters. The length of each numbered tube is described in Fig. 7. Z_{in} which is measured by blocking the receiver's port ($U = 0$) is plotted with Z_e (green line). (For interpretation of the references to colour in this figure legend, the reader is referred to the web version of this article.)

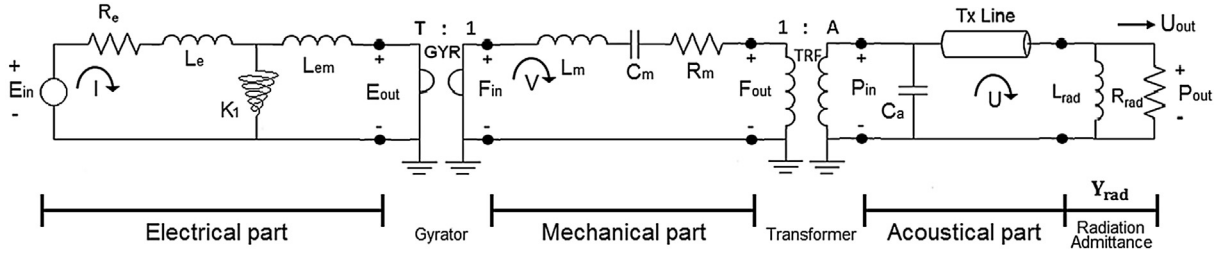

$$\begin{bmatrix} E_{in} \\ I \end{bmatrix} = \begin{bmatrix} 1 & R_e \\ 0 & 1 \end{bmatrix}\begin{bmatrix} 1 & sL_e \\ 0 & 1 \end{bmatrix}\begin{bmatrix} 1 & 0 \\ 1/K_1\sqrt{s} & 1 \end{bmatrix}\begin{bmatrix} 1 & sL_{em} \\ 0 & 1 \end{bmatrix}\begin{bmatrix} 0 & T \\ 1/T & 0 \end{bmatrix}\begin{bmatrix} 1 & sL_m \\ 0 & 1 \end{bmatrix}\begin{bmatrix} 1 & 1/sC_m \\ 0 & 1 \end{bmatrix}\begin{bmatrix} 1 & R_m \\ 0 & 1 \end{bmatrix}\begin{bmatrix} 1/A & 0 \\ 0 & A \end{bmatrix}\begin{bmatrix} 1 & 0 \\ sC_a & 1 \end{bmatrix}\begin{bmatrix} \cosh\left(\frac{Sl_t}{c}\right) & z_0\sinh\left(\frac{Sl_t}{c}\right) \\ \sinh\left(\frac{Sl_t}{c}\right)/z_0 & \cosh\left(\frac{Sl_t}{c}\right) \end{bmatrix}\begin{bmatrix} 1 & 0 \\ Y_{rad} & 1 \end{bmatrix}\begin{bmatrix} P_{out} \\ U_{out} \end{bmatrix}$$

Fig. 12. Final circuit model of the BAR, along with the equivalent ABCD matrix representation. The electrical and the mechanical circuits are coupled by a gyrator (GYR), while a transformer (TRF) is used for the coupling of the mechanical and the acoustical circuits. The input and output potentials for each section (E: voltage, F: force, P: pressure) are specified in the model. I (current), V (particle velocity), and U (volume velocity) represent the flow of each part. By computing the defined ABCD matrix and converting the result to the impedance matrix via Eq. (2), Hunt parameters of the transducer model may be calculated. The specific values for each components are listed in Table 1.

Because of measurement differences, this is not exactly the case. This resonant location can thus be interpreted as one of the most fundamental characteristics (eigen modes) of an electro-magnetic transducer.

Table 1
Specific parameters that are used for the suggested model (Knowles BAR ED7045). c is the speed of sound in the air (334.8[m/s]), $j\omega/c$, z_0, and l_t are the propagation function, specific characteristic impedance and length of the transmission line, respectively. GYR and TRF stand for the gyrator and the transformer. All model parameters were found by minimizing the RMS error between the model and electrical input impedance measurements of the receiver.

Electrical elements
$R_e = 195$ [Ω],
$L_e = 9$ [mH],
$K_1 = 27.5$ [Semi-Henry], $L_{em} = 52$ [mH]
GYR = 7.5
Mechanical elements
$C_m = 1.25e\text{-}3$ [F], $L_m = 4.3e\text{-}6$ [H], $R_m = 0.003$ [Ω]
TRF (1/Area) = $1/(2.4e^{-6})$
Acoustical elements
$C_a = 4.3e\text{-}15$ [F]
Tx Line: $z_0 = 1e9$ [kg/sec], $l_t = 1e\text{-}4$ [m]
Radiation impedance
$L_{rad} = 10^{10}$ [Acoustic-Henry], $R_{rad} = 10^{11}$ [Acoustic-Ohm]

6.2. Electrical impedance in vacuo

The acoustical part in the transducer model is removed for the vacuum case, while all the electrical and mechanical parameters in Fig. 12 during the experiments remain the same as the no-vacuum condition.

In Fig. 14, the simulated electrical input impedance results are expressed in two ways; the magnitude-phase and the polar plot (real vs. imaginary parts). For both the vacuum and the blocked port condition, the model (solid lines) and the experiment result (dashed lines) show reasonable agreement below ≈ 12[kHz].

The transducer model, including acoustical elements ('blocked' output port) is in red, and the model excluding acoustical elements (vacuum condition) is in blue. Both cases give similar shape, a pole, followed by a zero, with increasing frequency (≈890[Hz] in vacuum, ≈750[Hz] in blocked case). We conclude that the trapped air (between the diaphragm and the port of the receiver) influences the resonance by pushing it to higher frequencies due to the increased stiffness to mass ratio. Also because of the acoustical properties (including mechanical-acoustical coupling), the magnitude of the vacuum resonance is reduced by 1.9 dB compared to the blocking the receiver's output port (in air).

By looking at the polar plot (the right panel in Fig. 14), we can clearly see that the high frequency impedance is

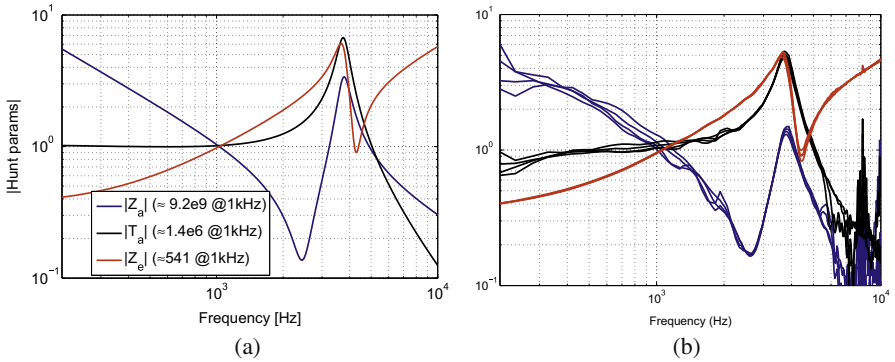

Fig. 13. Comparison of Hunt parameters (Z_e (red), T_a (black), and Z_a (blue)) from the model (a) and the measurements (b). Any significant differences between the model and the data occur above 6[kHz]. All parameters are normalized to their 1[kHz] values. (a) Hunt parameters from the model (b) Hunt parameters from measurement. (For interpretation of the references to colour in this figure legend, the reader is referred to the web version of this article.)

dominated by $\sqrt{s}$, clear evidence of the eddy-current, in the BAR. The many small loops appearing above 16[kHz] may be a measurement artifact, however the second resonance at 15 [kHz] is real.

6.3. Mechanical velocity measurement using laser in vacuo

As shown in Fig. 15, the mechanical velocity is also calculated from the transducer model and compared with the laser velocity measurement result. The model and the experiment are well matched below 10[kHz].

However small magnitude difference is observed; the laser measured data has about 1[dB] higher velocity at the FR and the low frequency area. There are some possible solutions to improve the model. First, when we make the laser measurement, one might focus on the laser beam in various places on the diaphragm and average out those data to see the overall velocity behavior of the diaphragm. It is true that we can get a slightly different velocity depending on the place where the laser is focused. As explained in method section, we put the laser's focus near at the rod (where the armature and the diaphragm is connected). And secondly, we could add or remove mechanical damping in the transducer model (i.e., increasing or decreasing the value of R_m in our model Fig. 12) relative to the present value. The problem below 200[Hz] is due to a very small hole that is burned into the diaphragm, to act as a very low frequency leak.

The mechanical velocity is calculated by assuming the force (F) in vacuum is zero. In reality, it is impossible to reach an absolute vacuum condition. Our experiment condition of 0.003[atm] seems adequate to understand the nature of the mechanical velocity of the transducer as the measurement gives a reasonable agrement with the model.

6.4. Thevenin pressure comparison

The model and measured Thevenin pressure are plotted in Fig. 16. Two indirect pressure estimation methods are used; one using the Hunt parameters, and the other using the simulation of our transducer model. There is a reasonable agreement among these measures up to 6–7[kHz]. The mathematical definitions of

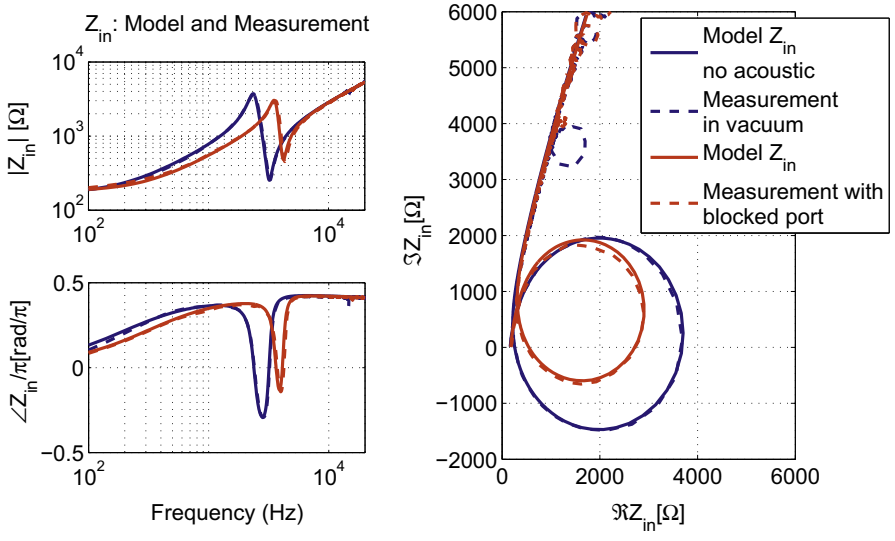

Fig. 14. Comparison the suggested model of Fig. 12 and real electrical input impedance measurement of a balanced armature hearing-aid receiver (Knowles, ED7045). Blue and red colors represent vacuum and non-vacuum (with air) conditions respectively. And the dashed lines stand for the experimental result whereas the single lines show the model results. For the vacuum experiment, the actual static pressure is less than 0.003[atm]. The left panel shows the magnitude and the phase of each condition and the real and imaginary parts of the same data are plotted in the right panel. Up to 23[kHz], the experimental data is in good agreement with the modeling result (The sampling rate is 48[kHz], therefore the maximum frequency is 24[kHz]). In the polar plot, when it goes to the higher frequencies, the impedance behaves as $\sqrt{s}$. (For interpretation of the references to colour in this figure legend, the reader is referred to the web version of this article.)

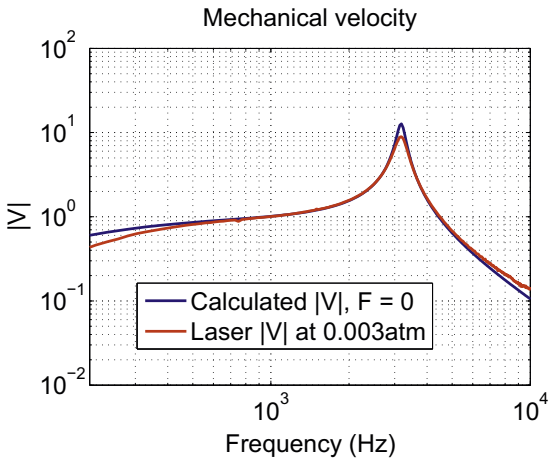

Fig. 15. Comparison of the diaphragm (mechanical) velocity between the transducer model and the laser measurement in vacuum, the pressure P is zero. For the model simulation, the acoustical part in Fig. 12 is not included. The laser measurement was performed after pumping out the air in the receiver. All values are normalized to one at 1[kHz].

these data are the Thevenin pressure per unit voltage (P/E), with a zero volume velocity ($U = 0$),

$$\left.\frac{P}{E}\right|_{U=0} = \left.\frac{T_a}{Z_e}\right|_{U=0}. \tag{25}$$

Note that P/I and P/E differ in the theoretical meaning as well as in the definition; $T_a \equiv \left.\frac{p}{I}\right|_{U=0}$ is one of the Hunt parameters, while the Thevenin pressure (per volt) in Eq. (25) is a more realistic experimental function, when one uses a voltage drive. For the comparison, the pressure data is divided by the voltage (E_{in}) across the two electrical terminals of ED7075 (A and B in Fig.10) when $U = 0$. The data from Section 3.1 is imported for E_{in}, assuming $U = 0$ at the port in the pressure measurement.

The green line in Fig. 16 shows the Thevenin pressure data derived from the ER-7C probe microphone. Other than the direct pressure measurement (green), all responses are derived from the

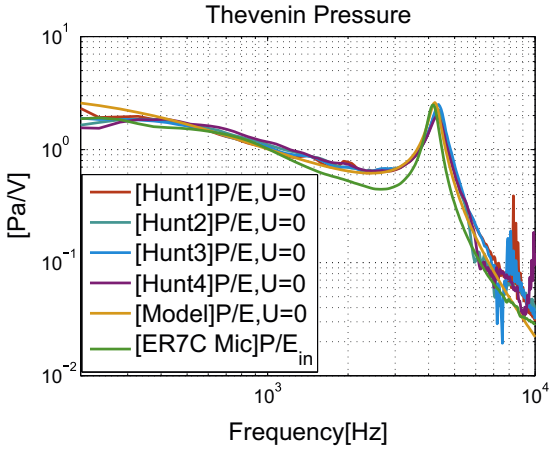

Fig. 16. Comparison of Thevenin pressure (per voltage) data from various sources. There are 6 different lines, the first 4 lines are calculated from the electrical experiments (Hunt parameters), and the orange colored line is estimated from the model. The last pressure data (in light-green) are taken from the pressure measurement and are divided by the electrical input voltage of the receiver. All data assume the blocked condition, $U = 0$ (see text). Every value is normalized to one at 1[kHz]. (For interpretation of the references to colour in this figure legend, the reader is referred to the web version of this article.)

Hunt parameter calculation introduced in the Appendix, using the 'electrical input impedance measurements' for acoustical loads.

7. Conclusion

In this study, we have discussed the critical elements of a BAR including a gyrator, and a semi-inductor along with the two-port network properties. Starting by solving for the Hunt parameters of the receiver, we have proposed a new circuit model which contains these elements, the gyrator and the semi-inductor. An intuitive design of an electromagnetic transducer has been enabled by using the gyrator thereby avoiding the mobility method, which can be confusing to explain or teach. Moreover, we have shown an improved high frequency matching by using the semi-inductors, especially for the electrical impedance,$Z_{\text{in}}(s)$.

The model has been verified by comparing the experimental data (obtained from laser, vacuum, and pressure measurements) to theoretical data (obtained through model simulations). All the comparisons are in good agreement with the experimental results, especially the electrical input impedance data introduced in Fig. 14, which matches to 23[kHz]. A major advantage of the proposed receiver model is that the acoustic Thevenin pressure can be calculated directly from electrical input impedance measurements.

Further study may improve the model for an improved match, such as the secondary loop as discussed in Section 6.2. Also one might consider a demagnetized transducer, allowing one to explore the nature of the electromagnetic transducer by looking at the Z_e is dominated only by the electrical parameters. Analyzing the f_p (introduced in Section 6.1) from various transducers could be another important topic for future study.

Acknowledgments

The authors are grateful to HSR group, especially Hanul Kim along with Daniel Warren, Chris Jones and Tom Miller at Knowles Electronics (Itasca, IL) for their gracious help with the vacuum and laser measurements.

Appendix A

Eq. (24) includes three unknown Hunt parameters (Z_e, Z_a and T_a) that we wish to find. In order to solve for three unknown parameters, 3 different electrical input impedances ($Z_{\text{in}|A}Z_{\text{in}|B}$, and $Z_{\text{in}|C}$) are measured corresponding to three known acoustic loads, A, B, and C. The load conditions differ in a length of the tubing, attached to the receiver's port. Each tube has different impedance denoted as $Z_{L|A}$, $Z_{L|B}$, and $Z_{L|C}$, where $Z_{L|A}Z_0\coth(a\cdot\text{tube\_length})$ (for the blocked-end tube, $U = 0$), Z_0 is the characteristic impedance of a tube, and a is the complex propagation function. Parameters a and Z_0 parameters assume viscous and thermal loss (Keefe, 1984). In 20° [C] room temperature, $c = 334.8$[m/s]. Define diameter of $Z_L|^A B_C \approx 1.4[mm]$

Substituting these for Z_L in Eq. (24):

$$\begin{aligned} Z_{\text{in}|A} &= \frac{E}{I} = Z_e + \frac{T_a^2}{Z_{L|A} + Z_a} \\ Z_{\text{in}|B} &= \frac{E}{I} = Z_e + \frac{T_a^2}{Z_{L|B} + Z_a} \\ Z_{\text{in}|C} &= \frac{E}{I} = Z_e + \frac{T_a^2}{Z_{L|C} + Z_a}. \end{aligned} \tag{A.1}$$

Given these three measured impedances, we can solve for Z_a, T_a, and Z_e via the following procedure:

1. Subtract two electrical impedance measurements to eliminate Z_e, such as

$$Z_{\text{in}|C} - Z_{\text{in}|A} = \frac{T_a^2}{Z_a + Z_{L|C}} - \frac{T_a^2}{Z_a + Z_{L|A}}. \tag{A.2}$$

2. Take the ratio of various terms as defined by Eq. A.2,

$$\left(\frac{Z_a - Z_{L|B}}{Z_{\text{in}|C} - Z_{\text{in}|A}}\right) = \left(\frac{Z_{\text{in}|A} - Z_{\text{in}|C}}{Z_{\text{in}|B} - Z_{\text{in}|C}}\right)\left(\frac{Z_{L|C} - Z_{L|B}}{Z_{L|C} - Z_{L|A}}\right).$$

From this we may solve for the first unknown Z_a,

$$Z_a = \frac{\left(Z_{\text{in}|A} - Z_{\text{in}|C}\right)\left(Z_{L|C} - Z_{L|B}\right)\left(Z_{\text{in}|C} - Z_{\text{in}|A}\right)}{\left(Z_{\text{in}|B} - Z_{\text{in}|C}\right)\left(Z_{L|C} - Z_{L|A}\right)} + Z_{L|B}. \tag{A.3}$$

3. Next we find T_a by substituting Z_a into Eq. (A.2)

$$T_a = \sqrt{\frac{\left(Z_{\text{in}|C} - Z_{\text{in}|A}\right)\left(Z_a + Z_{L|C}\right)\left(Z_a + Z_{L|A}\right)}{Z_{L|A} - Z_{L|C}}}. \tag{A.4}$$

4. Finally Z_e is given by Eq. (A.1)

$$Z_e = \left(\frac{T_a^2}{Z_{L|A} + Z_a}\right) - Z_{\text{in}|A}. \tag{A.5}$$

References

Bauer, B.B., 1953. A miniature microphone for transistor amplifiers. The Journal of the Acoustical Society of America 25, 867–869.

Beranek, L.L., 1954. Acoustics. McGraw-Hill.

Carlin, H.J., Giordano, A.B., 1964. Network Theory, an Introduction to Reciprocal and Nonreciprocal Circuits. (Englewood Cliffs NJ).

Dodd, M., Klippel, W., Oclee-Brown, J., 2004. Voice Coil Impedance as a Function of Frequency and Displacement.

Hunt, F.V., 1954. Electroacoustics: The Analysis of Transduction and Its Historical Background. Harvard University Press. Harvard University, Massachusetts.

Jensen, J., Agerkvist, F.T., Harte, J.M., 2011. Nonlinear time-domain modeling of balanced-armature receivers. Journal of Audio Engineering Society 59, 91–101.

Keefe, D.H., 1984. Acoustical wave propagation in cylindrical ducts: transmission line parameter approximations for isothermal and nonisothermal boundary conditions. Journal of the Acoustical Society of America 75, 58–62.

Killion, M.C., 1992. Elmer Victor Carlson: a lifetime of achievement. The Bulletin of the American Auditory Society 17, 10–21.

McMillan, E., 1946. Violation of the reciprocity theorem in linear passive electro-mechanical system. Journal of Acoustical Society of America 18, 344–347.

Mott, E.E., Miner, R.C., 1951. The ring armature telephone receiver. The Bell System Technical Journal, 110–140.

Tellegen, B., 1948. The gyrator, a new electric network element. Philips Research Reports 3, 81–101.

Thorborg, K., Unruh, A.D., Struck, C.J., 2007. A model of loudspeaker driver impedance incorporating eddy currents in the pole structure. Journal of Audio Engineering Society.

Van Valkenburg, M.E., 1964. Network Analysis, second ed. Prentice-Hall, Englewood Cliffs, NJ.

Vanderkooy, J., 1989. A model of loudspeaker driver impedance incorporating eddy currents in the pole structure. Journal of Audio Engineering Society 37 (3), 119–128.

Warren, D.M., LoPresti, J.L., 2006. A ladder network impedance model for lossy wave phenomena. The Journal of the Acoustical Society of America (abst) 119 (5), 3377.

Weece, R., Allen, J., 2010. A clinical method for calibration of bone conduction transducers to measure the mastoid impedance. Hearing Research 263, 216–223.

Wegel, R.L., 1921. Theory of magneto-mechanical systems as applied to telephone receivers and similar structures. Journal of the American Institute of Electrical Engineers 40, 791–802.